Sunflower Effect: Enhancement of Laser-Pulse-Induced Impulse in the Beam Incident Direction due to Surface Undulation

Yusuke Katagiri[1] and Akihiro Sasoh[1]

[1] Department of Aerospace Engineering, Nagoya University, Nagoya, Japan

E-mail: Akihiro.sasoh@mae.nagoya-u.ac.jp

Received xxxxxx
Accepted for publication xxxxxx
Published xxxxxx

Abstract

An impulse generated by laser ablation bas been implicitly assumed to be directed in the normal direction to the irradiation surface. In this study, however, the impulse induced by an Nd:YAG laser pulse with a wavelength of 1.064 μm irradiated on to a macroscopically flat aluminium plate ablator was enhanced in the direction of the laser beam incidence due to microscopic surface undulation, the characteristic height and pitch of which are tens of the beam wavelengths. The inner product of the incident laser beam vector and the normal vector to the surface is locally enhanced on the "sunny" side. In the vapor regime in which the impulse is an increasing function of the fluence, the effective fluence and the impulse component in the incident direction are enhanced. With repetitively irradiating laser pulses on to the same spot with a fluence of 4.5 J/cm^2 nominal to a macroscopically flat surface, the impulse gradually increased due to this "sunflower" effect, then became saturated. The momentum coupling coefficient in the saturation stage became an increasing function of the angle of incidence. This impulse performance will become considerably important in the application of laser ablation to the remote motion control or even deorbiting of space debris.

Keywords: laser ablation, pulsed laser, space debris, surface undulation

Nomenclature

A	laser beam cross-sectional area
$\mathbf{c}$	unit vector in the direction of laser beam incidence
$C_{\mathrm{m,BI}}$	momentam coupling coefficient in the laser beam incident direction
$\bar{d}$	characteristic peak-to-peak distance
E	laser pulse energy irradiated on to the ablator
$\bar{h}$	averaged height
$\mathbf{I}$	impulse vector
I_{BI}	impulse component in the laser beam incident direction
i_{FN}	impulse density, i.e., the impulse divided by the irradiation area, to a perfectly flat surface with a null angle of incidence.
N	total laser pulse number
$\mathbf{n}$	unit vector normal to the ablator surface
(x,y,z)	Eulerian coordinates (figure 1)
z_{S}	z value of ablator surface
ϕ	fluence (local value)
$\bar{\phi}$	fluence based on macroscopic projection area
$\bar{\phi}_{\mathrm{B}}$	fluence based on laser beam cross-sectional area
λ	wavelength of laser beam
θ	angle of incidence

1. Introduction

Laser ablation technology has a unique advantage of generating a thrust using a remote light source, which is extremely fascinating in space technology to remotely control the motion of orbital, noncooperative objects such as space debris [1]. Phipps et al. [2] proposed ORION project of deorbiting space debris with a ground-based laser system. Ebisuzaki et al. [3] proposed another system utilizing a Coherent Amplifying Network (CAN) laser [4] and a space telescope. The characteristics in laser-pulse-induced impulse, which is the time integration of a temporal thrust, have been investigated under an implicit assumption that it is generated normal to the irradiated surface [5,6]. Based on this assumption, experimentally measured impulse is characterized using the fluence (or intensity), pulse duration period, and wavelength of the laser pulse, and of the ablator material [7-10]. This assumption is physically valid if the surface is flat on the wavelength scale. However, in practice, such flatness is not guaranteed.

Wang [11] examined the integrated impulse characteristics after repetitively irradiating Nd:YLF laser pulses (wavelength, λ: 1047nm) on to an aluminum plate with various incident angles, exhibiting unusually large impulse with large incident angles, to which the above assumption was not applicable. So far, a clear physical explanation of such experimental results has not been obtained.

Many have reported that after being irradiated by laser pulses periodic pattern is formed on target surface. This is well known as "laser-induced periodic surface structure (LIPSS)." [12,13] LIPSS is observed on various materials, that is crystals [12,14-22], metals [20-25] and polymers [8,26] , with various laser wavelength, that is far-infrared [8,14], near-infrared [15,17,18,22,23,25,26], visible [16,19,22-24,26] and ultraviolet [21,26], and with various pulse duration, that is of the order of micro-second [8,14], nano-second [15,17-24], pico-second [16,21,25] and femto-second [13]. In most of related works, laser beam is irradiated normal to the target surface, that is with a null incident angle. Kaki and Horita [19], Lloyd et al. [27] obtained LIPSS even with an oblique incident angle. Theoretical works of LIPSS were also done [28,29].

In the present study, we examined the impulse characteristics in the beam incident direction induced by repetitive laser pulse irradiations on to a fixed spot, and associated them with ablator surface undulation.

2. Experimental Apparatus and Methods

The basic configuration of the experimental setup in this study was the same as of [10]. The ambient pressure in the vacuum chamber with an inner diameter of 0.7 m and a length of 2.2 m was set to 2 mPa with a turbo molecular pump (2000 L/s, TMP-2003LM, Shimadzu co.) backed by a rotary pump (533 L/s, T2033SD, A-VAC Industries Inc.). The impulse measurement was conducted with a newly developed torsional pendulum set in the vacuum chamber. The displacement near the end of its arm, at 507 mm from the flexure pivot as the fulcrum, was measured with a laser displacement sensor (resolution, 1 μm; IL-030, KEYENCE co.). The sensitivity of the pendulum was improved by more than 10 times by reducing its moment of inertia from 0.61 kg-m^2 to 0.042 kg-m^2 and replacing two flexure pivots (spring constant, k, of 0.096 N-m/rad) with a single, weaker one with k = 0.024 N-m/rad set on the lower side of the arm. For inducing ablation, we used an Nd:YAG pulse laser (λ = 1064nm; pulse width, 9±2 ns (FWHM); M^2= 3-4). An impulse was measured after each single laser pulse irradiation. The energy of a laser pulse ranging from 9.6 mJ to 190 mJ was irradiated on the plate surface through a plano-convex lens with a focal length of 500 mm. The irradiation surface of the aluminum plate was positioned 340 mm from the lens. The diameter of the incident laser beam on the ablator was 1.65 mm with a flat top intensity profile. The height distribution of the ablator surface was measured using a laser microscope (horizontal resolution: 0.277 μm, height resolution: 0.001 μm, VK-9710, KEYENCE co.).

A laser beam was irradiated normal to the pendulum arm and with an incident angle of θ to the aluminum plate (figure 1), which was varied by tilting the aluminum plate from 0 to 60 deg.. The plate was rotated by using the stepping motor by 27 deg. so that many series of experiments starting with a virgin surface were conducted.

To investigate the impulse characteristics, we used a 2-mm-thick, 30 mm × 30 mm square, macroscopically flat, aluminum plate (A1050, purity≧99.5 %) with its surface being left rough as was upon commercial delivery. In the following experiments, we measured I_{BI} (figure 1) after each pulse irradiation. The measurement was repeated after an interval of about 60-s. The averaged depth of the ablated spot after N= 10 was 1 μm at most [30,31], which was less than 0.1 % of the spot diameter. Therefore, the macroscopic deformation of the spot could be neglected.

Here, $\bar{\phi}$ is defined as the irradiated laser energy divided by a macroscopic, projection area irradiated by the laser beam. Note here that as seen in figure 1, the irradiated surface area equals the laser beam cross-sectional area divided by $\cos\theta$. We assume that I_{BI} is given by

$$I_{\mathrm{BI}} = I_{\mathrm{BI}}(\bar{\phi}, \theta, N) \tag{1}$$

$$\bar{\phi} = \bar{\phi}_{\mathrm{B}} \cos\theta \tag{2}$$

$$\bar{\phi}_{\mathrm{B}} \equiv \frac{E}{A} \tag{3}$$

Here, we neglect the influence of θ on the absorptance of the aluminium plate.

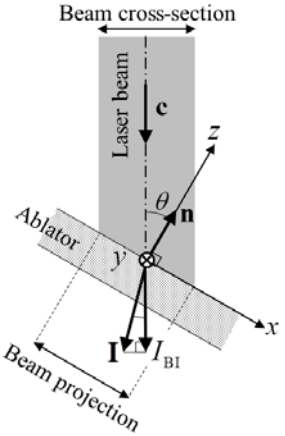

Figure 1. Definition of coordinates and vectors.

3. Results and Discussions

Figure 2 shows the variations of experimentally measured I_{BI} with N with a couple of values of $\bar{\phi}$ and θ. For each value of $\bar{\phi}$, three operation stages exist:

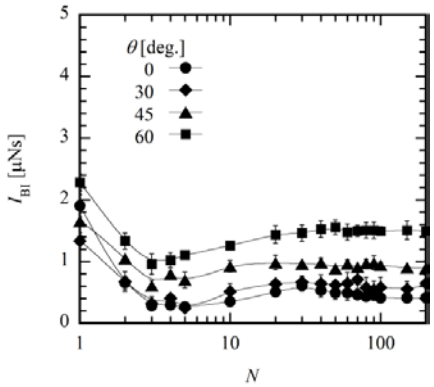

(a) $\bar{\phi} = 4.5$ J/cm^2

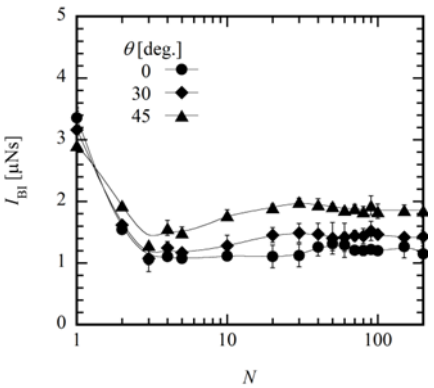

(b) $\bar{\phi} = 6.3$ J/cm^2

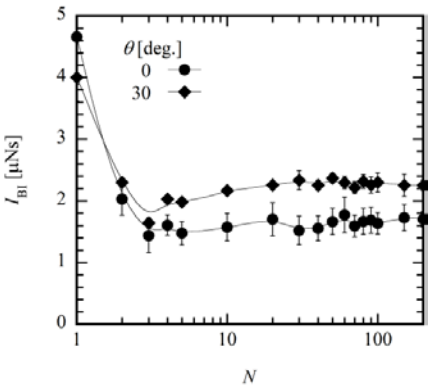

(c) $\bar{\phi} = 7.7$ J/cm^2

Figure 2. I_{BI} vs. N; symbol, ensemble average of experimental value; an error bar is twice as long as the corresponding standard deviation.

(1) Cleaning stage ($N \le 3 \sim 5$): I_{BI} rapidly decreased with increasing N. This characteristic commonly appears in the beginning of repetitive pulse laser ablation [8], and is claimed by contaminants including ablator material particles attached on to the rough surface. Such contaminants act as an additional propellant mass, thereby enhancing the impulse. Usually, the effect of the contaminants is avoided by conducting "cleaning" shots, in which laser pulses with a much smaller energy are irradiated. Yet, in this study, such cleaning shots were not conducted, but laser pulses with a constant energy were irradiated from the first shot. After a couple of laser pulse irradiations, I_{BI} had a minumum at $N = 3 \sim 5$. Since the impulse characteristics in this stage strongly depended on the contamination condition, which were difficult to control, in the followings the impulse characteristics in this stage will not be discussed.

(2) Enhancement stage ($3 \sim 5 \le N \le 30 \sim 50$): I_{BI} slowly increased with increasing N. This impulse enhancement and associated mechanisms will be analyzed in detail later.

(3) Saturation stage ($30 \sim 50 \le N$): I_{BI} almost became saturated to a constant value which depended on $\bar{\phi}$ and θ.

With a constant value of $\bar{\phi}$, if the irradiated surface was macroscopically flat without roughness in dimensions larger than λ, I_{BI} should be constant, independent of θ. However, as seen in figure 2, I_{BI} increased with increasing θ. This is qualitatively consistent with the results obtained by Wang [11], in which the impulse performance with a constant $\bar{\phi}_{\mathrm{B}}$ was experimentally measured. For example, as shown in figure 2(a), with $\bar{\phi} = 4.5$ J/cm^2 and N= 200 the impulse with $\theta = 60°$ is 3.6 times as large as that with $\theta = 0°$.

Figure 3 shows the laser microscope images with different θ and N. Figure 3(a) shows rough surface without

laser pulse irradiation, which was not pre-treated after the commercial delivery. With $\theta = 0$ and $N = 20$ (figure 3(b), humps with a diameter of the order of 18μm and a height of 6μm are formed. They are aligned somehow in random manner. With increasing N to 200 (figure 3(c)), with some of small humps observed in figure 3(b) being merged, both the diameter and the height became several times larger. With $\theta = 60$ deg. (figure 3(d) and (e)), the humps have longitudinal structure.

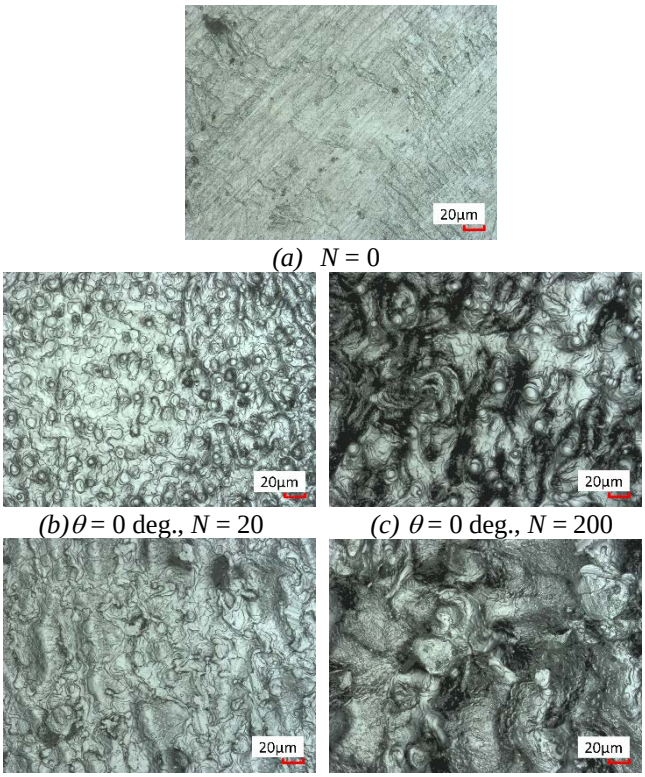

(a) $N = 0$

(b) $\theta = 0$ deg., $N = 20$ *(c)* $\theta = 0$ deg., $N = 200$

(d) $\theta = 60$ deg , $N = 20$ *(e)* $\theta = 60$ deg., $N = 200$

Figure 3. Laser microscope images of specimen surface, $\bar{\phi}$ = 4.5 J/cm^2.

Figure 4 shows examples of ablated surface profile measured using the laser microscope with $N = 20$. Here, we define the characteristic scales of the surface undulation. The characteristic height of undulation, $\bar{h}$, is defined as the doubled value of the root mean square (r.m.s.) of the z-coordinate of the ablator surface, z_s, in a surface profile measured using the laser microscope.

$$\bar{h} = 2\sqrt{\frac{\int_0^{\Delta y}\int_0^{\Delta x}\left(z_s - \bar{z}_s\right)^2 \mathrm{d}x\mathrm{d}y}{\Delta x \Delta y}} \tag{4}$$

$$\bar{z}_s = \frac{\int_0^{\Delta y}\int_0^{\Delta x} z_s \mathrm{d}x\mathrm{d}y}{\Delta x \Delta y} \tag{5}$$

Δx and Δy are the view widths of the specimen. $\bar{d}$, the characteristic value of the width of a hump, is evaluated by averaging over fifteen randomly-chosen, one-dimensional profiles cut in a profile.

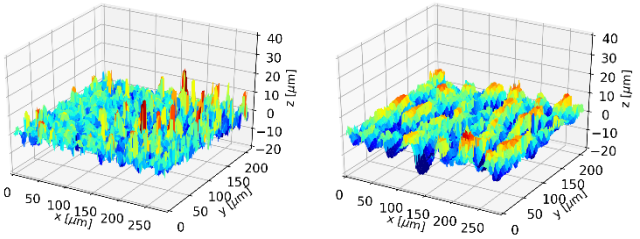

(a) $\theta = 0°$ *(b)* $\theta = 60°$.

Figure 4. Height distributions in a portion of 200 μm × 250 μm ablated surface area, $\bar{\phi}$ = 4.5 J/cm^2, N = 20.

Figure 5 shows the variations in the characteristic surface profiles with $\bar{\phi} = 4.5$ J/cm^2. The height distribution in the virgin surface was not characterized within the resolution of the laser microscope. Even after five irradiations (N=5), noticeable undulation appeared with $\bar{h}/\lambda = 1.9$ to 2.8, and then increased with N. At N =20, $\bar{h}/\lambda = 5.7$ to 7.4. $\bar{h}$ and $\bar{d}$ apparently increased further with further increase in N. The aspect ratio, $\bar{h}/\bar{d}$, also increased with increasing N, however remain smaller than 0.7 at most. Note that here that in the measurement, only the uppermost profile could be detected, cavities under uppermost surface are hidden even if they existed. Therefore, we analyze the relationship between the surface profile and the impulse performance only during the beginning of the undulation formation ($N \le 20$). In this range, as seen in figure 5, the value of $\bar{d}/\lambda$ varies in a narrow range between 17 and 21 wavelengths.

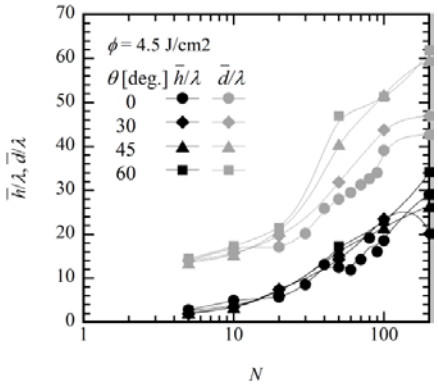

Figure 5. Variations of ablator surface profile with N, $\bar{\phi}$ = 4.5 J/cm^2.

Assuming that the impulse in the laser beam incident direction, I_{BI}, is obtained by the following geometrical relation.

$$I_{\mathrm{BI}}\left(\bar{\phi},\theta,N\right)=-\frac{A}{\Delta x\Delta y\cos\theta}\int_0^{\Delta y}\int_0^{\Delta x} i_{\mathrm{FN}}\left(\phi\left(x,y,N\right)\right)\mathbf{c}\cdot\mathbf{n}\left(x,y,N\right)\mathrm{d}x\mathrm{d}y \qquad (6)$$

in which the local fluence is given by

$$\phi\left(x,y,N\right)=-\bar{\phi}_{\mathrm{B}}\mathbf{c}\cdot\mathbf{n}\left(x,y,N\right) \qquad (7)$$

In equation (6), with a perfectly flat surface, $\mathbf{c}\cdot\mathbf{n}=-\cos\theta$; thereby, I_{BI} would become independent of θ. However, with $\mathbf{c}\cdot\mathbf{n}$ being varied due to surface undulation, I_{BI} does not have a constant value. Moreover, in the vapor regime [32], the impulse density $i_{\mathrm{FN}}(\phi)$ is an increasing function of ϕ. As seen in figure 3, in this study the periodicity on the ablated surface structure is weak; it is difficult to accurately evaluate I_{BI} for the following three reasons: (1) Due to the random profile, the integration in equation (6) needs to be done in the whole ablated area. However, the area of the laser microscope observation was rather small – about 2 % of the whole ablated area with θ = 0 deg. (2) In the concave regimes, the ablation pressure is enhanced by the confinement effect, which is not taken into consideration in equation (6). (3) An important characteristic appearing with microscopic structure is to enhance local electric field and then electron emission from the material, which is known as "field enhancement" [33-37]. This effect is expected to become strong when the characteristic height of the undulation becomes large. For these reasons, quantitative impulse evaluation warrant further investigations.

Figure 6 shows the variation of the momentum coupling coefficient in the laser beam incident direction defined by

$$C_{\mathrm{m,BI}}\equiv\frac{I_{\mathrm{BI}}}{E} \qquad (8)$$

As is usually obtained in the vapor regime, $C_{\mathrm{m,BI}}$ is an increasing function of $\bar{\phi}$. In principle, against the perfectly flat surface, $C_{\mathrm{m,BI}}$ should be independent of θ. For N=3, clear dependence of $C_{\mathrm{m,BI}}$ on θ was not obtained; the scatter was rather large presumably due to uncertainty in the condition of rough ablator surface. However, for N=200 $C_{\mathrm{m,BI}}$ increased with increasing θ. This is a surprising characteristic and the most important point of this paper. The ablator surface which experienced the undulation effectively increased the impulse performance in the beam incident direction. In principle, this "sunflower" effect should be obtained with other materials and laser conditions in the vapor regime in particular, and becomes considerably important in practical application of space laser propulsion including deorbiting and/or motion control of space debris.

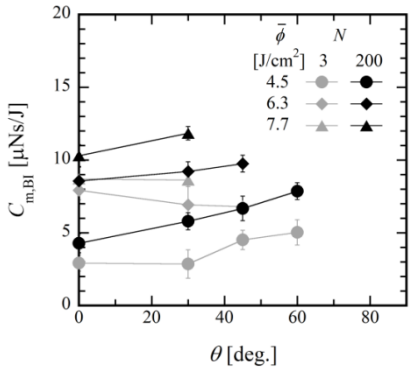

Figure 6. $C_{\mathrm{m,BI}}$ *vs.* θ.

4. Conclusions

In this study on the impulse performance of aluminium ablation against Nd:YAG laser pulses with λ = 1.064 μm, the impulse in the beam incident direction was enhanced because of the formation of ablator surface undulation with dimensions several or a few ten times larger than λ. The enhancement both of the local fluence and of the impulse component in the laser beam incident direction can account for this increment. This impulse performance has not been clarified from the macroscopic consideration of laser ablation impulse generation, and will be considerably important in the application of this technology to space debris motion control, for example.

Acknowledgements

This research was supported by the Japan Society for Promotion of Science as Grant-in-Aid for Scientific Research (A), 16H02426. The authors wish to thank the Technical Division at Nagoya University for their technical support and Mr. Vineet Poosarla for his technical assistance.

References

[1] Phipps C., Birkan M., Bohn W., Eckel H.-A., Horisawa H., Lippert T., Michaelis M., Rezunkov Y., Sasoh A., Schall W., Scharring S. and Sinko J. 2010 *Journal of Propulsion and Power* **26**, 609–37.

[2] Phipps C., Albrecht G., Friedman H., Gavel D., George E., Murray J., Ho C., Priedhorsky W., Michaelis M. and Reilly J. 1996 *Laser and Particle Beams* **14**, 1-44.

[3] Ebisuzaki T., Quinn M. N., Wada S., Piotrowski L. W., Takizawa Y., Casolino M., Bertaina M. E., Gorodetzky P., Parizot E., Tajima T., Soulard R. and Mourou G. 2015 *Acta Astronautica* **112**, 102–13.
[4] Soulard R., Quinn M. N., Tajima T. and Mourou G. 2014 *Acta Astronautica* **105**, 192–200.
[5] Pakhomov A. V. and Gregory D. A. 2000 *AIAA Journal* **38**, 725–7.
[6] Liedahl D. A., Libby S. B., Rubenchik A. and Phipps C. 2010 *AIP Conf Proc.* **1278**, 772-9.
[7] Phipps C. R., Turner T. P., Harrison R. F., York G. W., Osborne W. Z., Anderson G. K., Corlis X. F., Haynes L. C., Steele H. S., Spicochi K. C. and King T. R. 1988 *Journal of Applied Physics* **64**, 1083–96.
[8] Suzuki K., Sawada K., Takaya R. and Sasoh A. 2008 *Journal of Propulsion and Power* **24**, 834–41.
[9] Phipps C. R., Boustie M., Chevalier J.-M., Baton S., Brambrink E., Berthe L., Schneider M., Videau L., Boyer S. A. E. and Scharring S. 2017 *Journal of Applied Physics* **122**, 193103.
[10] Tsuruta H., Dondelewski O., Katagiri Y., Wang B. and Sasoh A. 2017 *Acta Astronautica* **136**, 46–54.
[11] Wang B. 2017 *Applied Physics Letters* **110**, 014101.
[12] Birnbaum M. 1965 *Journal of Applied Physics* **36,** 3688–89
[13] Bonse J, Hohm S, Kirner S V, Rosenfeld A and Kruger J. 2017 *IEEE Journal of Selected Topics in Quantum Electronics* **23,** 9000615
[14] Emmony D C, Howson R P and Willis L J. 1973 *Applied Physics Letters* **23,** 598–600
[15] Young J F, Sipe J E and Driel H M V. 1984 *Physical Review B* **30,** 2001–15
[16] Trtica M, Gakovic B, Radak B, Batani D, Desai T and Bussoli M. 2007 *Applied Surface Science* **254,** 1377–81
[17] Sun W, Qi H, Fang Z, Yu Z, Yi K and Shao J. 2014 *Applied Surface Science* **309,** 79–84
[18] Satapathy P, Panda R, Sahoo R, Shukla M K, Khatua L, Sahoo P K, Das R and Das S K. 2018 *Journal of Laser Micro/Nanoengineering* **13,** 146–9
[19] Kaki H and Horita S. 2005 *Journal of Applied Physics* **97,** 014904
[20] Hayat A, Latif A, Rafique M S, Khaleeq-Ur-Rahman M, Bhatti K A, Usman A and Rehman A. 2012 *Radiation Effects and Defects in Solids* **167,** 403–9
[21] Huynhand T. T. D. and Semmar N. 2017 *Surface TopogFaphy: Metrology and Properties* **5**, 035003
[22] Young J F, Preston J S, Driel H M V and Sipe J E. 1983 *Physical Review B* **27,** 1155–72
[23] Dauscher A, Feregotto V, Cordier P and Thomy A. 1996 *Applied Surface Science,* 410–4
[24] Tehniat S., Bashir S., Mahmood K. and Sharif A. 2018 *Laser and Particle Beams* 36, 427–441
[25] Aguilar-Morales A I, Alamri S and Lasagni A F. 2018 *Journal of Materials Processing Technology* **252,** 313–21
[26] Recktenwald T. and Mucklich F. 2003 *Prakt. Metallogr.* **40**, 614-637
[27] Lloyd R, Abdolvand A, Schmidt M, Crouse P, Whitehead D, Liu Z and Li L 2008 *Applied Physics A* **93,** 117–22
[28] Guosheng Z, Fauchet P M and Siegman A E. 1982 *Physical Review B* **26,** 5366–81
[29] Sipe J E, Young J F, Preston J S and Driel H M V. 1983 *Physical Review B* **27,** 1141–54
[30] Fishburn J., Withford M., Coutts D. and Piper J. 2006 *Applied Surface Science* **252**, 5182–5188.
[31] Sakai T. 2009 *Journal of Propulsion and Power* **25**, 406–614.
[32] Sinko J. E. and Phipps C. R. 2009 *Applied Physics Letters* **95**, 131105.
[33] Late D J, Singh V R, Sinha S, More M A, Dasgupta K and Joag D S. 2009 *Applied Physics A* **97,** 905–9.
[34] Zhao Q Z, Ciobanu F and Wang L J. 2009 *Journal of Applied Physics* **105,** 083103.
[35] Singh A, Shinde D, More M A and Sinha S. 2015 *Applied Surface Science* **357,** 1313–8
[36] Jalil S A, Bashir S, Akram M, Ahmed Q S and Haq F U. 2017 *Indian Journal of Physics* **91,** 953–65
[37] Akram M., Bashir S., Jalil S. A. Rafique S., Hayat A. and Mahmood K. 2018 *Materials Research Express* **5**, 025029